Study of the streamwise evolution of turbulent boundary layers to high Reynolds numbers

I. Marusic[1], K. A. Chauhan[2], V. Kulandaivelu[1], and N. Hutchins[1]

[1]Dept. of Mechanical Engineering, University of Melbourne, Parkville, VIC 3010, Australia

[2] School of Civil Engineering, University of Sydney, Sydney, NSW, 2006, Australia

We consider the streamwise evolution of zero-pressure-gradient turbulent boundary layers developing on the smooth floor of the Melbourne wind tunnel. The flat plate extends over 27 m, and three different tripping devices are used to set the initial conditions. The first trip consists of standard sand-paper, and the second and third trips consist of the addition of threaded rods of diameter 6 and 10 mm, respectively, that lead to "over-tripped" conditions. Fixed Reynolds number per metre U_∞/ν, where $U_\infty \approx 20$ m/s is the freestream velocity and ν is kinematic viscosity, is maintained with a well-established zero pressure gradient for all tripping configurations. As the boundary layer evolves along the length of the tunnel floor, the mean velocity profiles are found to approach a constant wake parameter Π (as suggested by Coles 1962) for all the three tripping configurations after a sufficient distance downstream of the tripping devices. The broadband turbulence intensities and higher order moments are found to show variations up the same streamwise distance, here corresponding to O(2000) trip-height lengths downstream of the trips. Further downstream the boundary layers appear to be independent of initial upstream condition and reach converged states. The discussion is aided by computations based on a modified approach originally described by Perry *et al.* (2002), where given an initial upstream mean velocity profile, mean flow parameters are computed for different streamwise stations. The results are shown to compare well with the experimental results.

1 Introduction

A long standing topic in the study of wall-bounded turbulent flows is to understand their scaling behaviour. This is required for both theoretical and practical reasons, and invariably the basis for evaluating a proposed scaling law relies on comparisons with empirical data. In the case of zero-pressure-gradient (ZPG) boundary layers these comparisons are conducted over a range of Reynolds numbers, as this is the assumed sole non-dimensional parameter that specifies the state of the boundary layer. However, comparisons of experimental data from different studies rely on an assumption that scaled results (that is, statistical measurements made non-dimensional with the appropriate scaling parameters) are equivalent provided the local Reynolds numbers are equivalent. Figure 1 shows schematically a simple example of this for a typical comparison in the same wind tunnel. The Reynolds number can be matched by varying a combination of U_∞, the freestream velocity, and x, the streamwise distance

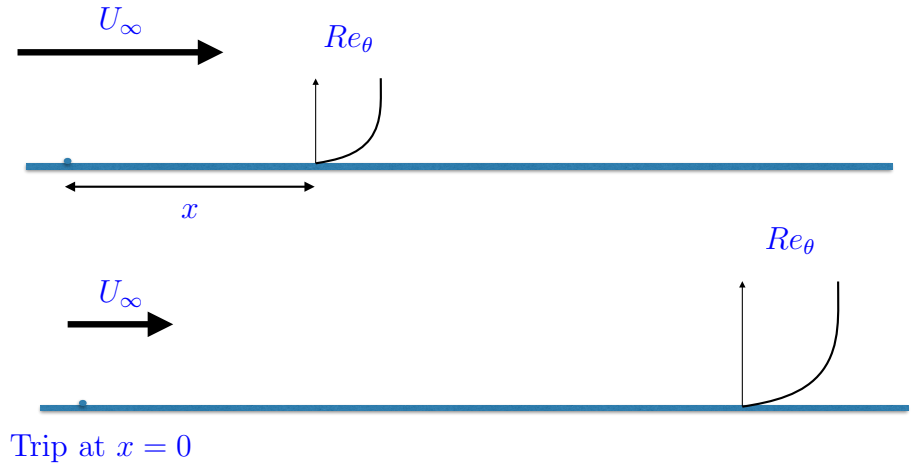

Figure 1: A schematic of two experiments. The local Reynolds number, Re_θ, is the same for both cases but the top case uses a higher velocity and shorter streamwise distance from the trip to achieve the required Reynolds number.

from the trip. When making such comparisons the local Reynolds number can be either the friction Reynolds number (also known as the Karman number) $Re_\tau = \delta U_\tau/\nu$, or the Reynolds numbers based on momentum or displacement thicknesses, $Re_\theta = U_\infty\theta/\nu$, $Re_{\delta^*} = U_\infty\delta^*/\nu$, respectively. Here, δ is the boundary layer thickness, U_τ is the skin-friction velocity, ν is the kinematic viscosity of the fluid, θ is the momentum thickness, and δ^* is the displacement thickness. Therefore, when comparing one experiment to another it is implicitly assumed that there exists a one-to-one correspondence between any of these local Reynolds numbers. The aim of this paper is to understand under what conditions these assumptions are valid, and under what conditions the effects of upstream trip and other initial conditions no longer play a role in defining the state of the boundary layer.

To someone new to the field it may seem strange as to why this is still a question given that these flows have been studied over many decades. The issue certainly is not new, but unfortunately although researchers have long recognised the importance of initial conditions in boundary layers, experimental challenges have remained and there have only been a small number of studies that have documented the streamwise evolution of boundary layers from fixed and carefully quantified initial conditions. One of the most rigorous studies performed in this area was by Erm & Joubert (1991) who investigated the effect of various tripping conditions on turbulent boundary layers for Reynolds numbers between $715 \leq Re_\theta \leq 2810$. Erm & Joubert (1991) proposed a technique for obtaining correctly stimulated turbulent boundary layers for a particular tripping device by changing the dimension of the trip iteratively until the measured Coles (1956) wake factor Π agrees with the Coles (1962) curve of Π versus Re_θ. For ZPG flows, then, all experiments should fall on one curve for Π versus a local Reynolds number. However, an extensive compilation of experiments by Chauhan & Nagib (2008), reproduced here in figure 2, shows that there exists considerable scatter in the available data, with a wide range of Π values reported for a given value of Re_{δ^*}. Such differences has lead to some investigators, such as Castillo & Johansson (2002), Johansson & Castillo (2001) and

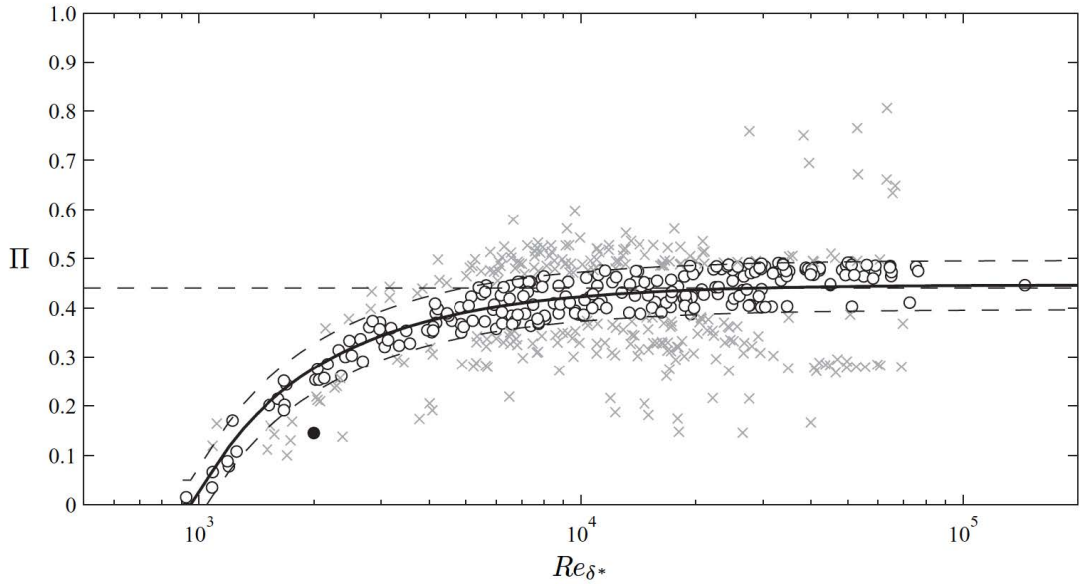

Figure 2: Compilation of experimental results for Coles wake factor versus $Re_{\delta*}$ from Chauhan *et al.* (2009). A total of 508 data points from a large number of experiments are shown of which 235 (circles) nominally agree with the solid line, which is obtained from an integration of the composite profile of Chauhan *et al.* (2009). Gray crosses represent profiles that have Π values beyond ± 0.05 of the solid line.

Castillo & Walker (2002) to produce new scaling laws where the initial conditions persistent for all time for boundary layers. While there are a number of reasons for the observed differences between different studies, we contend that the major differences in ZPG flows can be explained due to the insufficient evolution lengths in boundary layers and this is focus of the presented results. It is also noted that the trend of the curve shown in figure 2 where Π varies with $Re_{\delta*}$ has been described by Coles (1962) as a low-Reynolds number effect. Here, we will show that a more appropriate description is one based on an evolution effect resulting from the initial conditions set up by the trip and/or the initial inflow conditions.

1.1 Implications for big data

Presently it is not feasible to store all of the data that is generated in direct numerical simulations of evolving high Reynolds number wall-bounded flows, or to measure the full spatial domain of the flow in time-resolved experiments. The size of such datasets would simply be too onerous. Rather, decisions need to be made as to what given locations measurements are made in experiments, and what time-steps are kept in numerical simulations in order to recover the statistical quantities that are of interest. Therefore, there are obvious implications for the quantity of stored data that is required to properly document the evolution history of boundary layers. In the following we will study boundary layers with comparisons of statistics for flows that have evolved from three types of tripping conditions. By making detailed measurements at multiple streamwise locations for each flow we can determine over what streamwise distance the transients effects of the trips persist.

It is noted that the present paper should be seen as a supplement to the full paper of Marusic *et al.* (2015). Some of the main results are repeated here but additional results are presented in order to present a more complete report.

2 Experiments

Full details of the experimental facility and measurements are given in Marusic *et al.* (2015). The main features are use of the Melbourne wind tunnel, which was purpose built for this type of evolution study up to high Reynolds numbers. The boundary layer develops on the floor of the working section which is 27 m long, 1.89 m wide and 0.92 m high. The floor is made of aluminium plates of 6 m lengths that are polished to produce a hydrodynamically smooth surface. Careful upstream flow conditioning and a three-dimensional contraction, with a reduction area ratio of 6.2, produce a flow with a free-stream turbulence intensity ($\sqrt{\overline{u^2}}/U_\infty$) of 0.05% at the start of the working section, and in the range of 0.15-0.2% at $x \approx 18$ m. The working section is operated slightly above atmospheric pressure, and a series of adjustable slots and panels on the ceiling of the working section enables precise control of the streamwise pressure gradient. For all experiments presented here the coefficient of pressure C_p along the entire working section is constant to within $\pm 0.87\%$ (for all tripping configurations). For all cases, measurements were conducted with a nominal free-stream velocity of 20 m/s, with a reference Reynolds number per metre of $U_\infty/\nu = 1.295 \times 10^6$ m^{-1}.

The long development length of the working section produces thick boundary layers, which enables us to attain good spatial resolution with a conventional hot-wire probe design. In terms of spatial resolution, since the unit Reynolds number is matched everywhere, the only variation in the viscous scaled wire-length, $l^+ = lU_\tau/\nu$, occurs due to the weak variation in U_τ along the development length of the facility. At $x = 1.6$, the 0.54mm long sensing element yields $l^+ = 25.6$, falling to 22.3 at $x = 18$ m. Hence, the probes can be considered to be nominally matched in terms of viscous lengths ($l^+ = 24 \pm 2$, and precise values are given in table 1). Another important feature of the experiments was the use of a special calibration procedure to reduce drift. The hot-wire probes were statically calibrated against a Pitot-static tube positioned along the centreline of the tunnel in the undisturbed free-stream, and to account for calibration drift during the experiments, the probe was periodically traversed to the free-stream within the boundary layer profile measurement. At this free-stream excursion, the mean voltage measured by the hot-wire and the mean velocity measured by the Pitot-static tube provides an additional *re-calibration* point at various intervals during the boundary layer traverse. Effectively, this means that for every 6 measurements during the boundary layer traverse (which consisted of between 33 to 50 logarithmically spaced measurement stations), the probe is re-calibrated. This procedure leads to a considerable reduction in the scatter between repeat experiments and is described in detail by Talluru *et al.* (2014).

Three flow cases were studied corresponding to three different tripping configurations. All trips were introduced at the inlet to the working section (at $x = 0$ for the axis system used in this paper). The initial set of measurements was performed with the 'standard' tripping configuration, which consisted of a strip of P40 grit sand paper, of length 154 mm in the streamwise direction, and was chosen based on the criteria outlined by Erm & Joubert

Station	x (m)	Re_τ	Re_{δ^*}	Re_θ	δ (mm)	Π	U_∞^+	l^+
				SP40: Sandpaper (regular) trip				
1	**1.60**	2800	9800	7200	57.5	0.49	27.37	26.1
2	2.65	3600	12500	9300	75.2	0.48	27.97	25.5
3	3.75	4300	14900	11200	92.2	0.46	28.36	25.3
4	**4.75**	5100	16800	12700	108	0.41	28.54	25.3
5	6.30	6000	20600	15600	132	0.46	29.21	24.5
6	**7.50**	6700	22600	17200	150	0.43	29.36	24.1
7	10.00	8400	28400	21700	188	0.44	29.97	24.1
8	**12.80**	10500	33700	26100	237	0.38	30.25	23.9
9	17.50	13000	42800	33300	304	0.40	30.95	23.1
10	18.90	13400	45000	34900	319	0.43	31.15	22.7
				TR06: 6mm threaded rod				
1	**1.60**	3700	10700	8100	75.6	0.25	26.88	26.1
2	2.65	4900	13500	10400	101	0.21	27.40	25.8
4	**4.75**	6100	18400	14200	130	0.30	28.46	24.9
5	6.30	6800	22100	16900	148	0.39	29.20	24.3
6	**7.50**	7600	24500	18800	167	0.38	29.42	24.1
8	**12.80**	10700	35100	27100	244	0.40	30.41	23.2
-	15.50	12300	40000	31100	284	0.38	30.71	23.0
-	22.10	16300	53500	41800	385	0.40	31.51	22.4
				TR10: 10mm threaded rod				
1	**1.60**	8000	13900	11000	161	-	26.75	26.8
4	**4.75**	8700	20400	16100	184	0.07	28.13	25.5
6	**7.50**	9300	26200	20500	203	0.24	29.19	24.6
8	**12.80**	11800	36700	28600	269	0.34	30.36	23.6
-	15.50	13800	41700	32700	317	0.30	30.59	23.1
10	18.90	15400	48600	38100	361	0.36	31.13	23.0

Table 1: Experimental parameters for the SP40, TR06 and TR10 configurations respectively. Bold notation for streamwise distance x indicates that it is common measurement station for all three tripping configurations. For all cases, measurements were conducted with a nominal free-stream velocity of 20 m/s, with a reference Reynolds number per metre of $U_\infty/\nu = 1.295 \times 10^6$ m^{-1}.

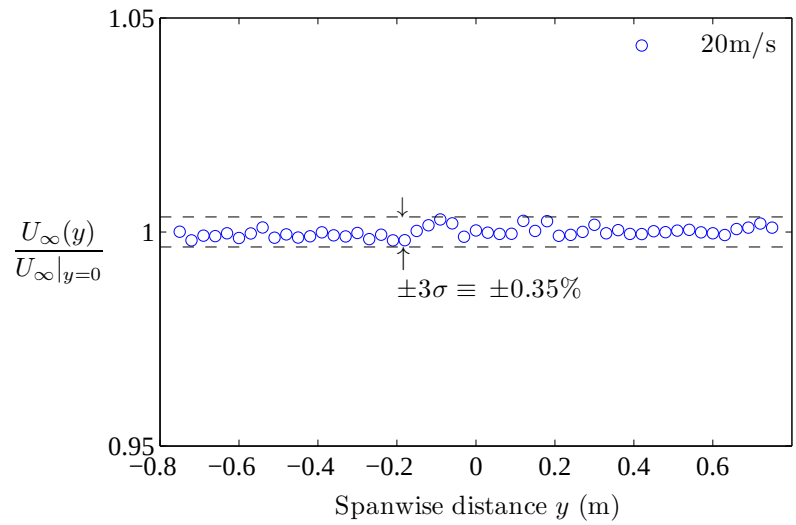

Figure 3: The relative spanwise variation of the freestream velocity $U_\infty = 20$m/s at $x = 10.4$ m downstream of the trip. The wall normal location is $z = 0.5$m.

(1991). The next two tripping configurations were deliberately chosen to over-stimulate the boundary layers. In these configurations, 6mm and 10mm diameter threaded rods were added at $x = 0$. We refer to the sandpaper and threaded rod configurations throughout as SP40, TR06 and TR10. Table 1 presents a summary of the main experimental parameters for each of the three cases. Here, $U_\infty^+ = U_\infty/U_\tau$ and in all cases U_τ, δ and Π are obtained by using the composite profile fit of Chauhan *et al.* (2009) using the log-law constants $\kappa = 0.384$ and $B = 4.17$.

Given the limited cross-sectional area of the working section ($1.89 \times 0.92\,\mathrm{m}^2$), compared to the very long length (27 m), careful attention was given to ensure that the boundary layers were nominally two-dimensional in the mean for the streamwise stations considered here. This is discussed in detail in Marusic *et al.* (2015), and figure 3 shows the results of Kulandaivelu (2012) who conducted a spanwise survey of free-stream velocity at $U_\infty \approx 20$ m/s at $x = 10.5$ m over a spanwise distance of 0.8 m either side of the tunnel center-line, and found the variation to be less than $\pm 0.35\%$ with no distinguishable slope in the velocity variation across the width of the boundary layer (corresponding to over $\Delta y \approx 8\delta$ at this streamwise station). The wind tunnel also contains corner fillets throughout the facility to minimise the effect of secondary flows in the corners of the wind tunnel. Comparisons of turbulence statistics at $x = 21$ m, with and without corner fillets in the working section revealed no discernible differences, providing further confidence that the boundary layers at all streamwise locations reported here are nominally two-dimensional in the mean.

Another important issue that should be clarified for this type of study is the appropriate Reynolds number for comparison based on streamwise distance. It has been proposed that a virtual origin, x_0, needs to be accounted for. That is, $Re_{(x-x_0)}$ should be used instead of Re_x. We consider this in figure 4 where we show boundary layer thickness versus streamwise distance for the three cases. It is noted that the boundary layers are abruptly tripped for the TR06 and TR10 configurations and hence the δ values for these two cases are significantly higher than the SP40 configuration. The low Reynolds number development of these

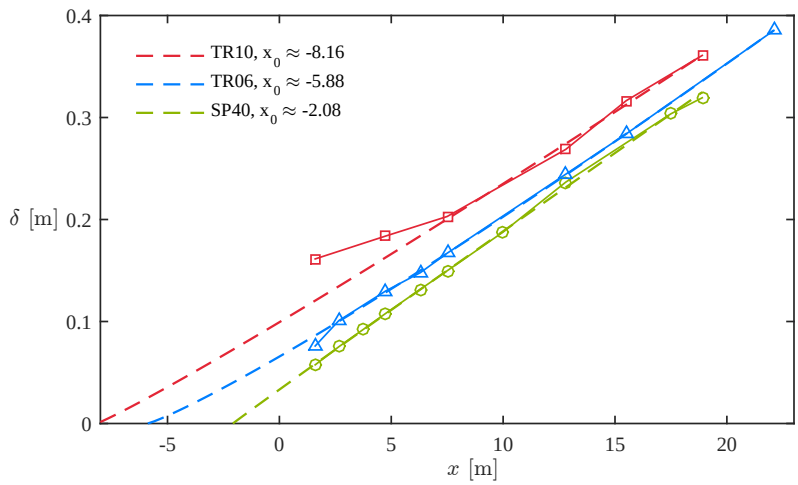

Figure 4: Boundary layer thickness versus streamwise distance for the three tripping conditions.

boundary layers is not self-similar (see Marusic *et al.* 2015) and therefore the virtual origin calculated in the figure 4 is not relevant. Here the objective is to examine the downstream influence of a particular tripping configuration on the flow measured at a particular streamwise distance on the floor. Hence, a streamwise variable x that is relative to the location where the transition trigger is placed is appropriate. This allows for a direct comparison of profile measurements at same the streamwise location as will be shown in the next section.

3 Results

In this section we compare the streamwise velocity statistics for the three cases. Figures 5(a) and 6(a) respectively show the normalised mean velocity and turbulence intensity profiles for four matched stations, thus corresponding to matched Re_x. The 'over-stimulated' cases TR6 and TR10 are clearly seen to be influenced at the initial stations compared to the 'canonical' SP40 case. For the mean velocity, the three configurations become identical further downstream as marked by the collapse in inner-scaled profiles. (The mean velocity-deficit profiles also agree when shown in outer scaling - see Marusic *et al.* 2015). The rate at which the over-stimulated boundary layers return to the canonical state depends on the type of trip. As expected, the TR06 configuration approaches the canonical state faster than the TR10. The same observations hold for the turbulence intensity results, where again by Station 8 (corresponding here to x=12.8 m) all the profiles nominally agree. The differences in the $\overline{u^2}^+$ profiles are seen at low Reynolds number, particularly in the outer region of the boundary layer, with the larger trip (TR10) resulting in larger deviations from canonical behaviour. Comparisons of spectra (shown in Marusic *et al.* 2015) reveal that the over-stimulated trips introduce large-scale disturbances into the boundary layer, which are prominent at low-Re. These large-scale disturbances reside predominantly in the outer part of the boundary layer, and likely originate or are amplified by the periodic shedding of the wake behind the rod. The presence of such energetic motions due to the abrupt tripping of

the boundary layer manifests as an outer peak in the spectrogram at low Re_x while at the same Re_x such large-scales are absent in the SP40 case. This artificial outer peak is different to the naturally occurring outer spectral peak that occurs at high Re in canonical ZPG flows. The remnants of the 'over-tripped' conditions are seen to persist at least until Station 8, at which position the non-canonical boundary layers (TR06 and TR10) exhibit a weak memory of their initial conditions only for the large-scales $O(10\delta)$.

One concern when making the above comparisons is the accuracy of determining U_τ for the over-tripped configurations, especially at low Reynolds numbers. In the absence of direct measurement of U_τ we rely on a composite velocity formulation that describes the mean velocity from the wall to the outer edge of the boundary layer. Chauhan *et al.* (2007) compared U_τ estimates from the composite profile formulation with direct measurements and found an agreement within $\pm 2\%$ for data at $Re_{\delta^*} < 10000$. Also, Chauhan *et al.* (2009) found that fitted U_∞^+ values are accurate within $\pm 1.5\%$ even for low Reynolds number data, i.e. $Re_{\delta^*} < 10,000$ when compared with U_∞^+ obtained from the integral skin-friction relation of Monkewitz *et al.* (2007) which is calibrated using oil-film interferometry data. Hence using the composite fit approach to determine U_τ at the initial stations seems reasonable. Further, the fitting algorithm considers equal weighting for all measured data. Therefore any non-canonical characteristics of the flow that are present in the mean velocity (in the inner, outer or both regions) will be accounted for in the fitting procedure. This results in the non-equilibrium influences to appear in the form of variations in U_τ, Π or δ compared to the canonical case of SP40. Non-equilibrium influences in ZPG flows were also illustrated using the parameters obtained from the composite velocity profile by Chauhan *et al.* (2009). To further check this, we plot U/U_∞ versus z in figure 5(b). In this form, figure 5(b) is free of any fitted parameters (U_τ or δ) and provides a direct comparison of momentum at a fixed x location between the three trip configurations. At the initial station we observe clear differences in the mean velocity throughout the boundary layer. Further downstream these differences are only seen in the outer region of the profiles. In the dimensional form, figure 5(b) clearly shows that the near-wall region of the over-stimulated flow recovers the earliest to match the canonical mean flow behaviour of the SP40 configuration. Similarly, we have utilised the outer scaling of U_∞^2 to compare $\overline{u^2}$ versus the dimensional wall-normal distance in figure 6(b). Here we again see that the three trip configurations have different levels of $\overline{u^2}$ at particular z throughout the layer at the initial stations. The differences diminish with streamwise distance and by Station 8 the $\overline{u^2}$ profiles agree well with each other in the near wall region while slight differences are observed in the outer region near $z \approx 15\,\mathrm{cm}$. This comparison again indicates that the transition by the threaded rod most significantly influence the outer region of the flow and the disturbances in the outer region persists downstream while the near-wall region recovers earlier to the canonical behaviour.

Higher-order statistics were also considered. Figures 7 and 8 show the comparisons respectively for even and odd higher-order moments of u up to tenth order. The even moments are presented in the form $(\overline{u^{2p}})^{1/p}$ following the work of Meneveau & Marusic (2013) who showed that even moments represented in this way have a logarithmic behaviour with distance from the wall in the log region of fully developed ZPG flows, and this is seen to be the case for the SP40 profiles. Comparison between the profiles in figures 7 and 8 and figure 5 indicate that the recovery length required for the statistics to become independent of the trip is not depen-

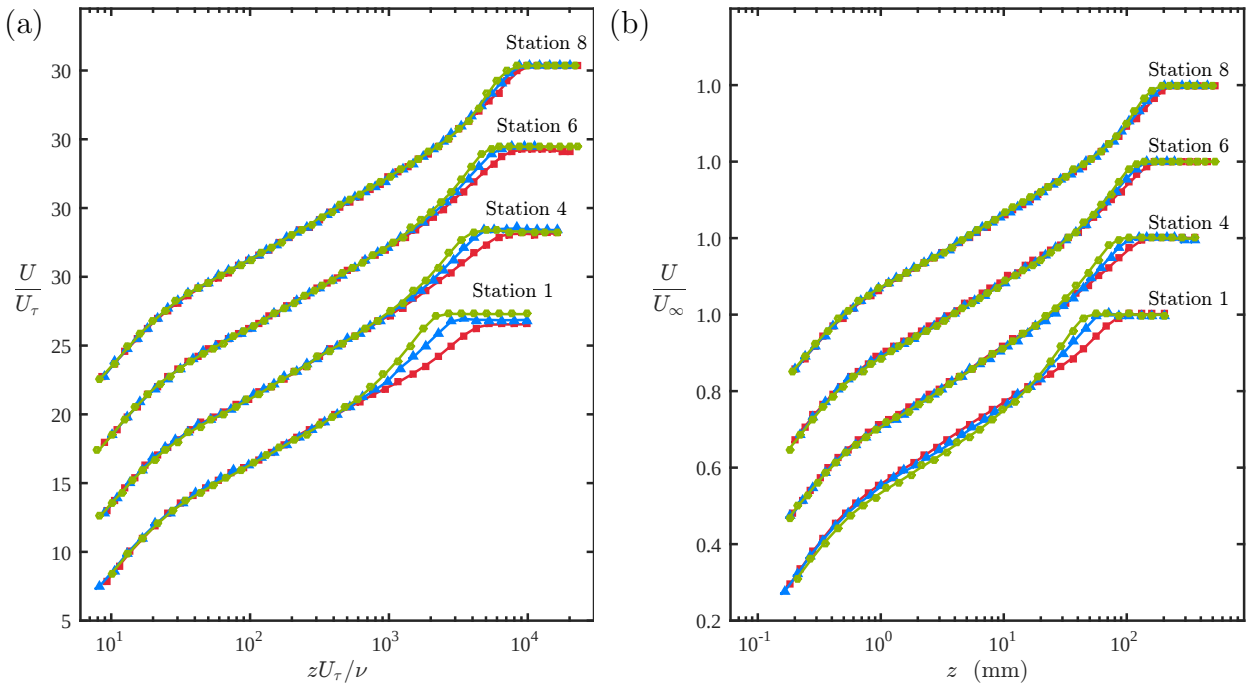

Figure 5: Comparison of mean velocity profiles for the three trips at four streamwise locations. '●', SP40; '▲', TR06; '■', TR10. Note the vertical shift in profiles. (a) with inner scaling; (b) where mean velocity is scaled with freestream velocity.

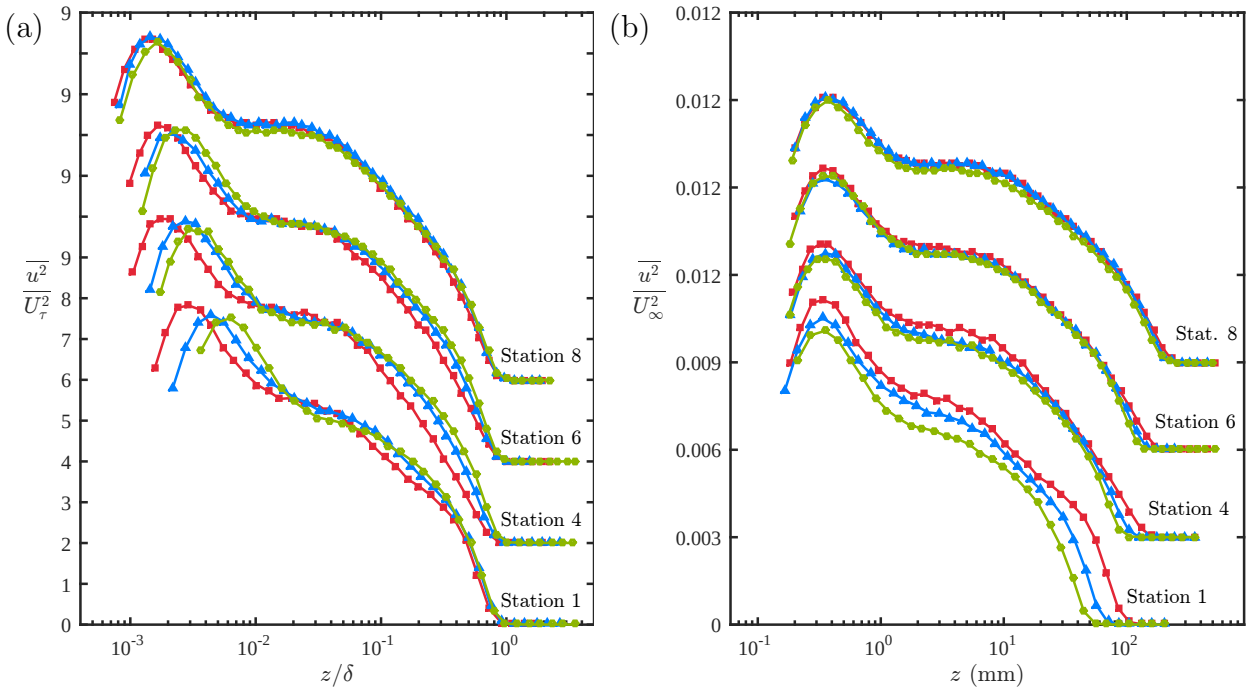

Figure 6: Comparison of streamwise turbulence intensity profiles for the three trips at four streamwise locations. '●', SP40; '▲', TR06; '■', TR10. Note the vertical shift in profiles. (a) with outer scaling; (b) scaled with freestream velocity.

dent on the order of the statistic (at least not up to tenth order), with all statistics nominally agreeing by Station 8. This suggests that while the larger trips introduce additional length scales into the flow, these perturbations and interactions relax as the boundary layer evolves downstream, and once they have decayed to the point of no longer influencing the mean velocity profiles, their effect also appears to be negligible for the higher-order statistics. This finding implies that in order to determine if a flow has sufficiently recovered from a trip and reached a canonical ZPG boundary layer state, only information about the evolution of the mean velocity profile is required. This is particularly advantageous as a reliable computation scheme can be developed for mean flow evolution, and this is considered in the following section.

4 Computing boundary layer evolution

Here we compute the streamwise evolution of the mean flow parameters for a ZPG boundary layer using the computational scheme outlined in Marusic *et al.* (2015). The approach uses the hypothesis that the mean velocity-defect profile is uniquely described by a two parameter family. In addition, a relation between the mean flow and shear-stress parameters is required to close the system of equations. The equations that govern the streamwise evolution of a turbulent boundary layer can be found after considerable algebra by using the momentum integral and differential equations, the mean continuity equation, and the log law of the wall and Coles (1956) law of the wake. A more detailed explanation is given in Perry *et al.* (1994), Perry *et al.* (2002), Jones *et al.* (2001) and Perry *et al.* (2002). A closure formulation is required and this is based on the limited empirical data available in the literature where the streamwise evolution of the boundary layer is fully documented.

The results of the computational scheme for the SP40, TR6 and TR10 cases are shown in figure 9 together with the data presented in Marusic *et al.* (2015) in addition to the data of Nagib *et al.* (2006) in the NDF facility at IIT. Overall the scheme is seen to agree well with all the experimental data. Here, $H = \delta^*/\theta$ is the shape factor and $C_f = 2(U_\tau/U_\infty)^2$ is the friction coefficient. It can be seen that though the local parameters such as the Reynolds number Re_x is matched (for the sake of Reynolds number similarity), different mean flow parameters (Π, H, C_f) can be obtained, and there is no guarantee that there is a one-to-one correspondence between local Reynolds numbers depending on the evolution state. The good fit of the computational scheme gives some confidence in evaluating the state of evolution for boundary layers.

All ZPG boundary layers are then expected to evolve to an equivalent form where Reynolds number similarity holds, provided the Reynolds number is sufficiently high, and the larger the trip is above the ideal trip size the longer the boundary layer will need to recover. However, it is not clear *a priori* how long this will take and how far downstream of the trip this will occur. The computational approach used here can provide this information and appears to be a valuable tool towards determining whether a given ZPG boundary layer is of a canonical form.

The authors gratefully acknowledge the Australian Research Council for the financial support of this project. We also thank Prof. Hassan Nagib for sharing the NDF data taken by Chris

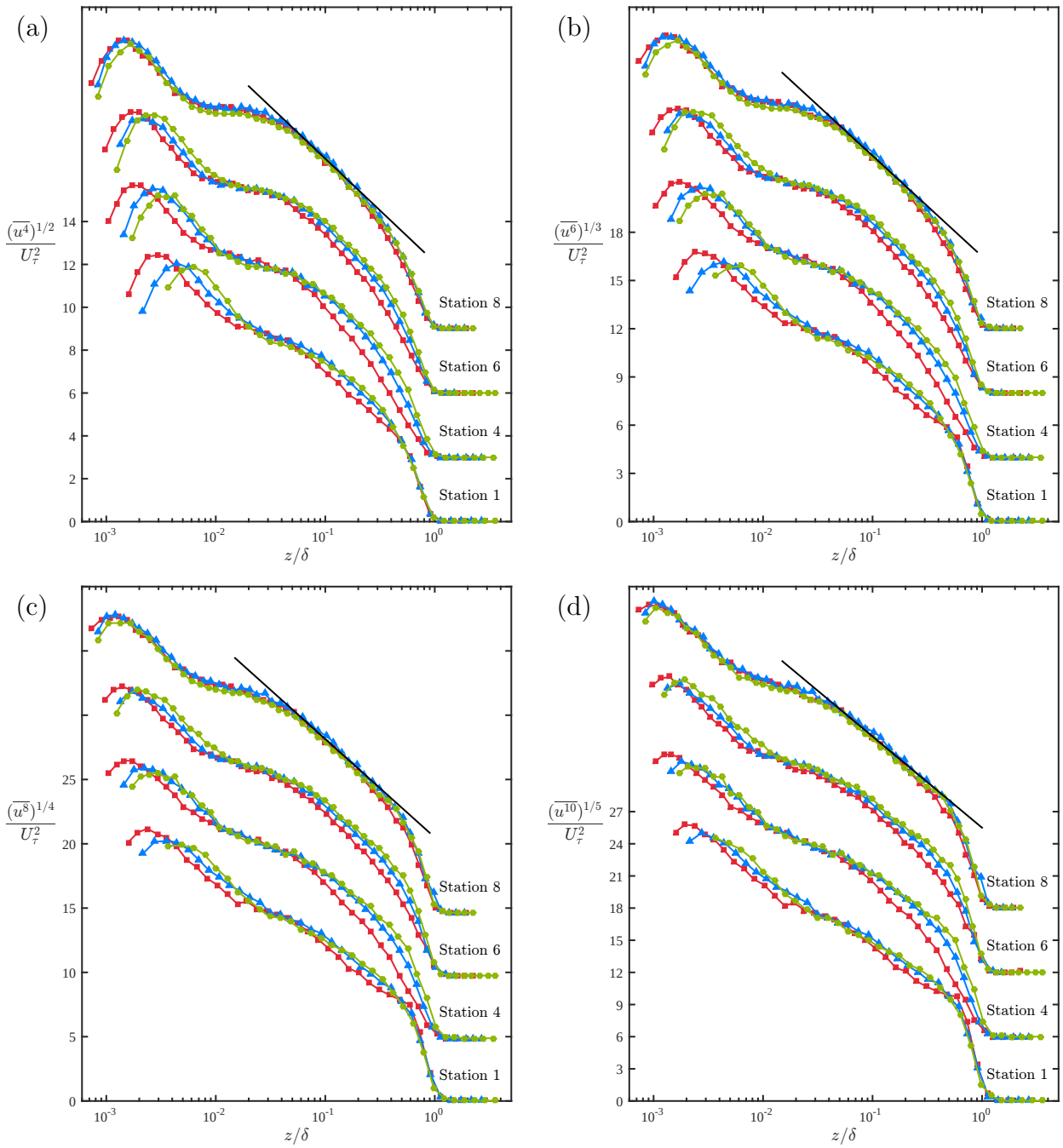

Figure 7: Comparison of even higher-order moments for the three trips at four streamwise locations. '●', SP40; '▲', TR06; '■', TR10. Note the vertical shift in profiles.

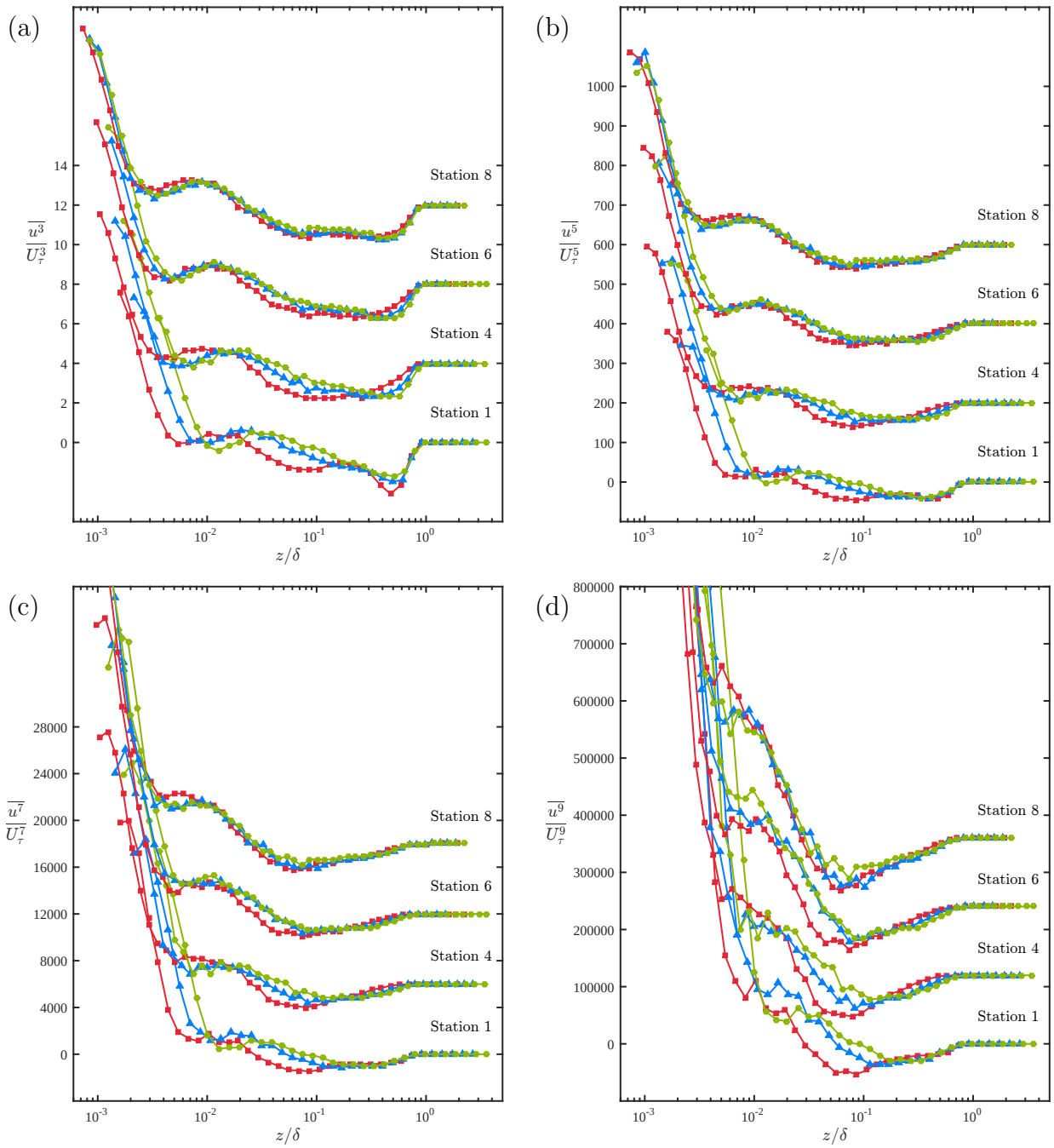

Figure 8: Comparison of odd higher-order moments for the three trips at four streamwise locations. '●', SP40; '▲', TR06; '■', TR10. Note the vertical shift in profiles.

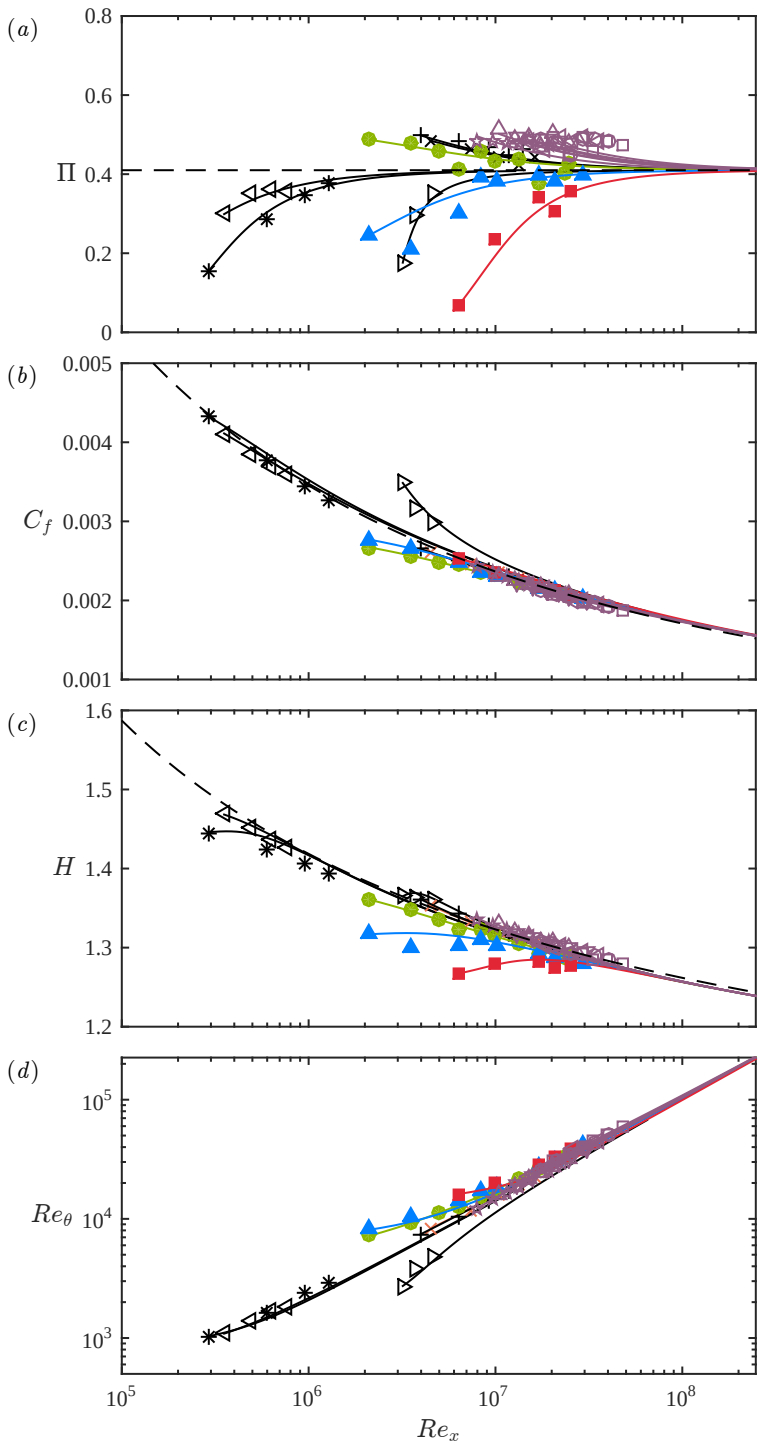

Figure 9: Comparison of experimental boundary layer parameters with computed evolution. (a) Π versus Re_x. Dashed line is the asymptotic limit of Π according to the definition of Chauhan *et al.* (2009); $\Pi \to 0.42$. (b) C_f versus Re_x. Dashed line is Schlichting's fit, $C_f = [2\log_{10}(Re_x) - 0.65]^{-7/3}$ (c) H versus Re_x. Dashed line is $H = (1 - 7.1/\sqrt{2/C_f})^{-1}$. (d) Re_θ versus Re_x. Purple coloured symbols are the data of Nagib *et al.* (2006). A description of the other datasets and further description of the dashed curves is given in Marusic *et al.* (2015).

Christophorou.

References

Castillo, L. & Johansson, T. G. 2002 The effects of the upstream conditions on a low Reynolds number turbulent boundary layer with zero pressure gradient. *J. Turb.* **3** (31), 1–19.

Castillo, L. & Walker, D. 2002 Effect of upstream conditions on the outer flow of turbulent boundary layers. *AIAA J.* **40** (7), 1292–1299.

Chauhan, K., Nagib, H. & Monkewitz, P. 2007 On the composite logarithmic profile in zero pressure gradient turbulent boundary layers. In *Proceedings of the 45th AIAA Aerospace Sciences Meeting and Exhibit, Reno, NV, Paper No. AIAA*, , vol. 532, pp. 1–18.

Chauhan, K. A. & Nagib, H. M. 2008 On the development of wall-bounded turbulent flows. In *IUTAM Symposium on Computational Physics and New Perspectives in Turbulence*, pp. 183–189. Springer.

Chauhan, K. A., Nagib, H. M. & Monkewitz, P. A. 2009 Criteria for assessing experiments in zero pressure gradient boundary layers. *Fluid Dyn. Res.* **41**, 021404.

Coles, D. E. 1956 The law of the wake in the turbulent boundary layer. *J. Fluid Mech* **1**, 191–226.

Coles, D. E. 1962 The turbulent boundary layer in a compressible fluid. Appendix A: A manual of experimental boundary-layer practice for low-speed flow. *Tech. Rep.* R-403-PR. USAF The Rand Corporation.

Erm, L. P. & Joubert, P. N. 1991 Low-Reynolds-number turbulent boundary layer. *J. Fluid Mech.* **230**, 1–44.

Johansson, G. & Castillo, L. 2001 LDA measurements in turbulent boundary layers with zero pressure gradient. In *Proc. 2nd Int. Symp. Turbulent Shear Flow Phenomena, Stockholm, Sweden*.

Jones, M. B., Marusic, I. & Perry, A. E. 2001 Evolution and structure of sink-flow turbulent boundary layers. *J. Fluids Mech.* **428**, 1–27.

Kulandaivelu, V. 2012 Evolution of zero pressure gradient turbulent boundary layers from different initial conditions. PhD thesis, University of Melbourne.

Marusic, I., Chauhan, K. A., Kulandaivelu, V. & Hutchins, N. 2015 Evolution of zero-pressure-gradient boundary layers from different tripping conditions. *J. Fluid Mech.* (In Press).

Meneveau, C. & Marusic, I. 2013 Generalized logarithmic law for high-order moments in turbulent boundary layers. *J. Fluid Mech.* **719**, R1.

Monkewitz, P. A., Chauhan, K. A. & Nagib, H. M. 2007 Self-contained high Reynolds-number asymptotics for zero-pressure-gradient turbulent boundary layers. *Phys. Fluids* **19**, 115101.

Nagib, H. M., Christophorou, C. & Monkewitz, P. A. 2006 High Reynolds number turbulent boundary layers subjected to various pressure-gradient conditions. In *IUTAM Symposium on One Hundred Years of Boundary Layer Research*, pp. 383–394. Springer.

Perry, A. E., Marusic, I. & Jones, M. B. 2002 On the streamwise evolution of turbulent boundary layers in arbitrary pressure gradients. *J. Fluids Mech.* **461**, 61–91.

Perry, A. E., Marusic, I. & Li, J. D. 1994 Wall turbulence closure based on classical similarity laws and the attached eddy hypothesis. *Phys. Fluids* **6** (2), 1024–1035.

Talluru, K. M., Kulandaivelu, V., Hutchins, N. & Marusic, I. 2014 A calibration technique to correct sensor drift issues in hot-wire anemometry. *Meas. Sci. Tech.* **25** (10), 105304.